Contents lists available at ScienceDirect

Chemical Engineering Research and Design

journal homepage: www.elsevier.com/locate/cherd

Modelling of the spray drying process for particle design

Ivana M. Cotabarren[a,*], Diego Bertín[a], Mariela Razuc[a,b], M. Verónica Ramírez-Rigo[a,b], Juliana Piña[a]

[a] Department of Chemical Engineering, PLAPIQUI, Universidad Nacional del Sur, CONICET, Camino La Carrindanga Km. 7, (8000), Bahía Blanca, Argentina

[b] Department of Biology, Biochemical and Pharmacy, Universidad Nacional del Sur, San Juan 670 (8000), Bahía Blanca, Argentina

ARTICLE INFO

Article history:
Received 27 July 2017
Received in revised form 20 December 2017
Accepted 4 January 2018
Available online 12 January 2018

Keywords:
Spray drying
Modelling
Atomization
Inhalable particles

ABSTRACT

Spray drying is widely applied in many industries, such as the pharmaceutical, food, detergents, polymers, to convert liquids in solid particles. However, it still requires continuous innovation in order to provide more sophisticated particles, which are difficult to design by using only empirical approaches. In this context, a steady-state mathematical model for a co-current spray dryer is developed to give a more phenomenological insight in the production of inhalable particles. The model includes mass, energy and momentum balances for both particulate and gaseous phases. Particularly, and as a model inhalable compound, ciprofloxacin hydrochloride (CIP) aqueous solutions are studied. Several experimental data, obtained in a Mini-Spray Dryer B-290, BÜCHI, were available. In addition, droplet size measurements were carried out by using laser diffraction. The effect of the binary nozzle operating conditions on the mean droplet size was analyzed and a correlation to predict the mean Sauter diameter was established. The experimental data are used to fit and validate the proposed model. The validated model is used to perform parametric studies in order to evaluate the effect of the main process variables on the final product properties (e.g., particle size and density, powder moisture content) and to track key powder attributes for pulmonary administration.

1. Introduction

Within the process industry, it is common to find unitary operations involving particulate systems, such as drying, granulation, grinding, mixing, crystallization, size classification, etc. They are part of a wide range of industries, from fertilizers and food production to pharmaceutical and mineral processing (Balliu, 2005; Christofides et al., 2007). Although about 60% of the chemical industry produces products in the form of particulate solids (Boukouvala et al., 2013; Christofides et al., 2008), these processes still operate with less efficiency than those that handle gases and liquids and, therefore, with little control of the product attributes because there are only few laws that can govern and describe their behaviour (Bell, 2005; Dobry et al., 2009). Recognized this lack of understanding, there is currently a large research activity worldwide, although concentrated in a small number of groups, tending to generate fundamental knowledge that allows the development of particles with defined properties and continuous improvement of the production processes.

Currently, the production of particulate solids with desired characteristics (among others, size, morphology, fluidity) is based on previous experience. The design of the units is mainly done by trial and error, while the control of processes is limited to the ability of operators (Burggraeve et al., 2013; Fung et al., 2006; Halstensen et al., 2006). This, almost exclusively, empirical approach involves not only laborious experiments with high development times, high costs, large waste gen-

* Corresponding author.
E-mail address: icotabarren@plapiqui.edu.ar (I.M. Cotabarren).
https://doi.org/10.1016/j.cherd.2018.01.012

Nomenclature

A	parameter in Walzel's correlation (Eq. (1)) [–]
A_a	area of the nozzle annulus [m^2]
A'	parameter in Eq. (25) [–]
ALR	air to liquid ratio [kg_{air}/kg_{liquid}]
B	parameter in Walzel's correlation (Eq. (1)) [–]
cp_a	air heat capacity [J/kg_{air} K]
cp_s	solid heat capacity [J/kg_{solids} K]
cp_v	vapour heat capacity [J/kg_{vapour} K]
$\overline{cp}_v$	average vapour heat capacity [J/kg_{vapour} K]
C	parameter in Walzel's correlation (Eq. (1)) [–]
C_D	drag coefficient [–]
d_{32}	Sauter mean diameter of droplets/particles [m]
d_{43}	volumetric mean diameter of droplets/particles [m]
d_{aer}	particle aerodynamic mean diameter [m]
d_{air}	boundary layer thickness of the surrounding air [m]
d_L	diameter of the liquid orifice [m]
d_p	droplet/particle mean diameter [m]
d_{p0}	droplet mean diameter at z_0 [m]
d_v	chamber wall thickness [m]
D_c	chamber diameter [m]
D_{eff}	diffusion coefficient of water vapour in the air [m^2/s]
F_{at}	atomization air volumetric flowrate [NL/h]
F_l	liquid feed flowrate [m^3/s]
k	ideal gas compressibility constant [–]
k_a	air thermal conductivity [W/m K]
k_v	glass thermal conductivity [W/m K]
m_s	mass of dry solids in the droplet [kg_{solids}]
$\dot{m}_v$	rate of evaporation from the droplet [kg_{water}/m^2 s]
$\dot{M}_a$	dry-air mass flowrate (drying and atomization air) [kg_{air}/s]
$\dot{M}_{ad}$	drying dry-air mass flowrate [kg_{air}/s]
$\dot{M}_{aat}$	atomization dry-air mass flowrate [kg_{air}/s]
$\dot{M}_l$	liquid feed mass flowrate [kg_{liquid}/s]
$\tilde{M}_a$	air molecular mass [kg_{air}/mol]
$\tilde{M}_w$	water molecular mass [kg_{water}/mol]
N_t	total number of droplets that enter the chamber [–]
N_u	Nusselt number [–]
Oh	Ohnesorge number [–]
P	atmospheric pressure [Pa]
P_v	vapour pressure [Pa]
Pr	Prandt number [–]
Q_0	gas volumetric flowrate upstream the nozzle exit [m^3/s]
R	universal constant of gases [–]
Re	Reynolds number [–]
RH	relative humidity [–]
T_0	temperature of the atomization gas upstream the nozzle exit [K]
T_a	air temperature [K]
T_{a0}	air temperature at z_0 [K]
T_{ad}	drying air inlet temperature [K]
T_{amb}	ambient temperature [K]
T_{out}	outlet air temperature [K]
T_p	droplet/particle temperature [K]
T_{p0}	droplet/particle temperature at z_0 [K]
U	global heat transfer coefficient [W/m^2 K]
v_a	air velocity [m/s]
v_p	droplet/particle velocity [m/s]
v_{p0d}	droplet/particle velocity at z_0 [m/s]
V_{p0}	droplet initial volume [m^3]
We	gas Weber number [–]
W_p	mass of water by mass of solids in the droplets [kg_{water}/kg_{solids}]
W_{p0}	mass of water by mass of solids in the droplets at z_0 [kg_{water}/kg_{solids}]
W_{pc}	critical moisture content [kg_{water}/kg_{solids}]
W_{peq}	equilibrium moisture content [kg_{water}/kg_{solids}]
X_w	droplet water mass fraction [$kg_{water}/kg_{droplet}$]
Y_b	relative humidity of the bulk air, dry basis [kg_{water}/kg_{air}]
Y_{b0}	relative humidity of the bulk air at z_0, dry basis [kg_{water}/kg_{air}]
Y_{sat}	maximum amount of liquid that can be absorbed by the surrounding air, dry basis [kg_{water}/kg_{air}]
z_p	axial distance from the nozzle [m]
z_0	axial position of the nozzle [m]

Greek symbols

α	heat transfer coefficient [W/m^2 K]
β	mass transfer coefficient of water vapour through air [kg_{air}/m^2 s]
γ_L	liquid surface tension [kg_{water}/s^2]
ΔH_{ev}	water latent heat of vaporization [J/kg_{water}]
μ_a	air viscosity [kgair/m s]
μ_L	liquid viscosity [kg_{liquid}/m s]
ρ_a	air density [kg_{air}/m^3]
ρ_L	liquid density [kg_{liquid}/m^3]
ρ_p	droplet/particle density [$kg_{droplet}/m^3$]
$\rho_{p,R}$	particle relative density [–]
ρ_{p0}	droplet/particle density at z_0 [$kg_{droplet}/m^3$]
ρ_s	solid density [kg_{solid}/m^3]
ρ_w	water density [kg_{water}/m^3]

eration and operations distant from the optimal points, but also considerable difficulties in ensuring the quality of the product (Vehring, 2007). Indeed, the particles final properties depend on the formation phenomena that occur in the production processes, which involve both operating and formulation variables (Patel and Chen, 2005; Vicente et al., 2013). Consequently, it is expected that the development of knowledge that provides a theoretical framework for particle design will contribute greatly to obtaining particulate products with controlled attributes.

Among the numerous existing processes for obtaining particulate materials, spray drying is used frequently and in a wide variety of industries, predominantly food and pharmaceutical, for its simplicity, ease of operation, feasibility of scaling and the ability to produce in one step and continuously, particulate systems containing various compounds (Sosnik and Seremeta, 2015). According to the application, it allows obtaining micro and nanoparticles, generally spherical and monodisperse, as dense, hollow, porous, encapsulated, etc. particles (Handscomb et al., 2009a). Despite the flexibility offered by this technology, control of particle size and morphology is critical (Vicente et al., 2013). Indeed, regardless of the application, proper tuning of numerous process and

formulation variables is required to achieve the desired characteristics (Vehring, 2007). The adjustable parameters of the spray-drying technique are related to the process, the liquid feed and the equipment (Handscomb et al., 2009a; Zbicinski, 2017). The main ones are the following: flowrate of liquid feed and drying gas, gas inlet temperature, concentration, viscosity, density, surface tension of the liquid feed, solvent boiling point, co-current or counter-current flow and atomizer geometry (Sosnik and Seremeta, 2015). Changes in these parameters lead to variations in particle size, process yield, particles morphology, crystalline state, moisture content and density, among others (Kemp et al., 2016; Sosnik and Seremeta, 2015).

Within the pharmaceutical industry, spray drying is used in the preparation of solid dispersions, manufacture of excipients, drying or encapsulation of active ingredients and, more recently, in the production of particles to be administered by inhalation (Lyu et al., 2017). Indeed, the particle size that demand inhalable products is at the lower limit of the spray drying technology (Kemp et al., 2013; Maltesen et al., 2008; Patel et al., 2014). However, only scarce information is available on how to control the formulation and operating variables to achieve given product properties, specifically a desired particle size distribution (PSD) (Kemp et al., 2013).

In this context, the aim of this work is to contribute to the design of inhalable particles produced by spray drying and to a more robust operation by combining process modelling and simulation with experimentation. Particularly, and as a model inhalable compound, ciprofloxacin hydrochloride (CIP) aqueous solutions are studied. The CIP is an antibiotic of the fluoroquinolones group used in the treatment of numerous infections (MedlinePlus, 2017) including respiratory infections in cystic fibrosis, anthrax and chronic obstructive pulmonary disease (COPD). Although frequently given as oral and injectable forms, the inhalation route could be an interesting alternative to direct CIP to the site of action (local therapy) or absorption (systemic therapy), minimizing its adverse effects (Adi et al., 2010a,b). The CIP solutions were dried by using a Mini Spray Dryer B-290, BÜCHI (Flawil, Switzerland) equipped with a high performance cyclone and a design of experiments was implemented to evaluate the relative importance of the process parameters and the accuracy of the proposed model.

2. Mathematical model

Spray drying is a common method for drying a liquid stream (solution or suspension) by a hot drying medium (usually air), which provides the liquid with sufficient energy to evaporate the solvent (preferably water) in order to obtain a particulate product of commercial interest. As shown in Fig. 1a, the spray drying in a co-current scheme involves the following stages: atomization of the liquid feed in the drying chamber (1) together with the drying air (2), contact between the atomized droplets and the gas to allow solvent evaporation (3) and separation of the particles from the drying gas (4, 5 and 6) (Kuriakose and Anandharamakrishnan, 2010).

Spraying is done by means of an atomizer where the fluid feed is broken into a large number of small droplets. There are different types of atomizers, the pressure and binary nozzles (also known as two-fluid or pneumatics nozzles) are the most used in the pharmaceutical industry for their simplicity, easy cleaning, flexibility and the ability to atomize various feeds (Vicente et al., 2013). Binary nozzles, where the liquid to be atomized circulates by a central channel and the atomizing gas (often air) through the surrounding annulus (see Fig. 1b), are preferred to produce fine particles (i.e., below 20 μm) (Kemp et al., 2013). Atomization is a key step and experimental evidence shows a high correlation between droplet and particle size (Vicente et al., 2013).

Within the drying chamber, the droplets are subjected to a wide variety of phenomena, which combine to define the quality of the final product (Schmitz-Schug et al., 2016). In general, the drying process of the droplets can be divided into two stages. In the first drying stage, the droplets contact the hot gas and gain sensible heat that leads to evaporation of the solvent and a subsequent droplet contraction. The second drying stage begins with the formation of a crust on the surface of the droplets, which become wet particles (Mezhericher et al., 2008). If a rigid crust is formed, the particles will not further shrink during drying, although they may become fragmented. If the crust is flexible, the particle size may decrease further or even increase if the liquid is heated above its boiling point. Consequently, and according to the droplets morphology (solution and/or suspension, nature and concentration of the constituent materials) and the operating conditions of the drying process (that govern the ratio between the solvent evaporation rate and the solute mass transfer by diffusion), particles of various morphologies can be obtained (Bück et al., 2012; Handscomb et al., 2009b; Kemp et al., 2013; Pinto et al., 2014; Seydel et al., 2006; Vehring, 2007). A micro-scale model able to describe all the variety of morphologies that the particles can take after drying does not exist (Tsotsas, 2015); however significant progress in modelling has been achieved, as recent literature shows (Mezhericher et al., 2010; Tran et al., 2017; Vehring et al., 2007). Independently of the used micro-scale model, an important feature is the ability to connect the results of the solid-phase formation process (e.g. particle porosity) to process variables (Tsotsas, 2015).

The spray-dryer model proposed in this work includes a mathematical representation of the liquid feed atomization in order to obtain a relationship between the droplets mean size and operating parameters, and a one-dimensional model considering variation in the axial direction to describe the drying of the formed droplets inside the unit chamber.

2.1. *Atomization model*

As previously mentioned, the droplet size distribution from the two-fluid atomizer is key on the spray drying process, but cannot be predicted from first principles (Pinto et al., 2014). In this type of nozzles, the ratio of the mass flowrates of the atomizing gas (usually, air) and liquid feed, air to liquid ratio (ALR), is often used as a characterization parameter (Hede et al., 2008; Kemp et al., 2013). Actually, by appropriate manipulation of the atomization conditions (mainly ALR and liquid feed properties) it is possible to achieve reasonable control over particle size (Maltesen et al., 2008).

Numerous correlations have been reported to estimate the mean droplet diameter, although relatively few for binary nozzles (Kemp et al., 2013). Typically, the Sauter mean diameter d_{32}, is predicted. For binary nozzles (Fig. 1b), Walzel (1993) proposed the following semi-empirical relationship (Pacheco et al., 2016; Walzel, 2012):

$$d_{32} = A\, d_L \left[\frac{\mathrm{We}}{\left(1 + \frac{1}{\mathrm{ALR}}\right)^2} \right]^B (1 + C\,\mathrm{Oh}) \quad (1)$$

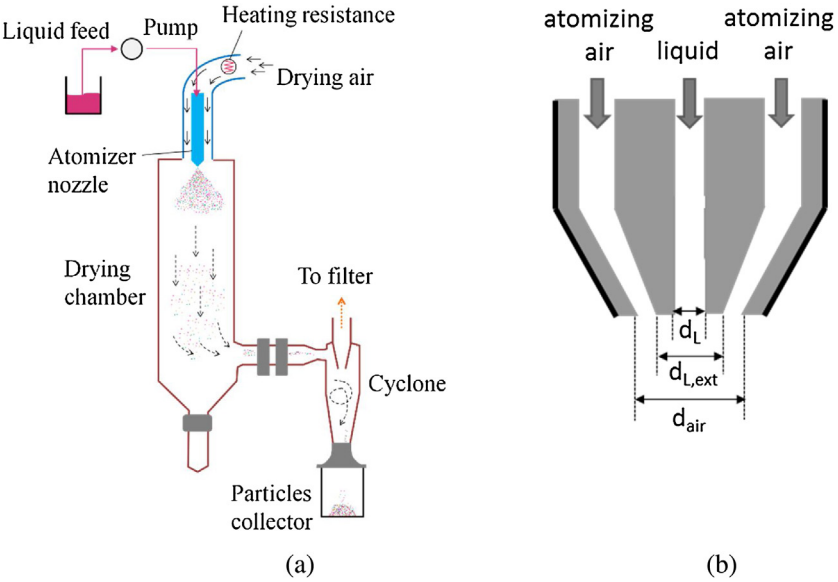

Fig. 1 – (a) Schematic representation of a spray dryer. (b) Configuration of an externally mixing two-fluid nozzle.

Two important dimensionless numbers, which are widely used in droplet size characterization studies, appear in Eq. (1): the gas Weber number, $We = v_a^2 \rho_a d_L / \gamma_L$, given by the ratio of air dynamic pressure to liquid capillary pressure and the Ohnesorge number, $Oh = \mu_L / \sqrt{\gamma_L \rho_L d_L}$, that accounts for the relative importance of stabilizing viscous forces to surface tension ones (Pacheco et al., 2016). Therefore, the Sauter mean diameter estimated by Walzel's correlation depends on the diameter of the liquid orifice (d_L), the atomization air velocity and density (v_a and ρ_a), the liquid surface tension, density and viscosity (γ_L, ρ_L and μ_L), the ALR and three fitting parameters (A, B and C).

The gas velocity through the annulus is calculated from the upstream volumetric flowrate, by considering the compressibility of gases. By assuming a one-dimensional, stable and isoentropic process, and that air behaves like an ideal gas, mass and energy balances can be combined with thermodynamic relationships to obtain (Smith et al., 1997):

$$v_a = \frac{Q_0}{A_a}\left[1 + \frac{\tilde{M}_a(k-1)}{2RkT_0}\left(v_a^2 - \frac{Q_0^2}{A_a^2}\right)\right]^{1/(k-1)} \quad (2)$$

where Q_0 is the gas volumetric flowrate upstream the nozzle exit, A_a the area of the annulus, $\tilde{M}_a$ the air molecular mass, k the compressibility constant, R the universal constant of gases and T_0 the temperature of the atomization gas upstream the nozzle exit (it is assumed that the temperature does not change considerably). If v_a is higher than the speed of sound, it is instead computed by Eq. (3), valid for a Mach number of 1 (Smith et al., 1997):

$$v_a = \sqrt{\frac{2RkT_0}{(k+1)\tilde{M}_g}} \quad (3)$$

2.2. Drying model

The model proposed in this contribution considers the following assumptions:

(a) The drying medium is preheated air and the solvent of the sprayed solution is water.
(b) The drying air and the atomized liquid are co-current.
(c) Steady-state for both, the air and the droplets/particles phases.
(d) Plug flow for both, the air and the droplets/particles phases (i.e., variations in the radial direction of mean droplet/particle size, droplet and air temperature, droplet and air moisture and droplet and air velocity are neglected) (Edrisi Sormoli and Langrish, 2016).
(e) Droplets are spherical.
(f) The driving force for evaporation is the difference between the air humidity considering saturation at the droplet surface (by neglecting the CIP content) and the relative humidity of the bulk air (Negiz et al., 1995).
(g) Moisture and temperature profiles inside the droplets are neglected.
(h) Agglomeration and breakage of droplets are neglected.
(i) Heat transfer between droplets and air is considered.
(j) The spray dryer exchanges heat with the surrounding air through the chamber wall.
(k) The chamber is considered to be a cylinder (the actual spray-dryer geometry is more complex, see Fig. 1a).

2.2.1. Solid phase balances

The humidity balance in the droplet (W_p, dry basis) is given by:

$$\frac{dW_p}{dz} = -\frac{\pi d_p^2 \dot{m}_v}{v_p m_s}, \quad W_p(z_0) = W_{p0} \quad (4)$$

where z is the axial distance from the nozzle, m_s is the mass of dry solids in the droplet, v_p and d_p are the velocity and diameter of the droplet, $\dot{m}_v$ is the rate of evaporation from the droplet by unit of surface area and W_{p0} is the mass of water by mass of solids in the droplets at the nozzle, estimated from the droplet initial composition ($W_{p0} = X_w/(1 - X_w)$, being X_w the droplet water mass fraction). The rate of evaporation is a function of the mass transfer coefficient of water vapour through air (β) and the driving force for the mass transfer, which is given by the difference between the relative humidity of the air at the droplet temperature (Y_{sat}, dry basis, maximum amount of

liquid that can be absorbed by the surrounding air) and the relative humidity of the bulk air (Y_b, dry basis):

$$\dot{m}_v = \beta(Y_{sat} - Y_b) \tag{5}$$

$$Y_{sat} = \frac{P_v \tilde{M}_w}{(P - P_v)\tilde{M}_a} \tag{6}$$

where P corresponds to the atmospheric pressure, P_v is calculated through Antoine's equation and β is estimated as a function of the heat transfer coefficient (α):

$$\beta = \frac{\alpha \rho_a D_{eff}}{k_a} \tag{7}$$

with D_{eff} as the diffusion coefficient of water vapour in the air and ρ_a and k_a as the density and conductivity of air, respectively. For the heat transfer coefficient, the correlation stated by Ranz and Marshall (1952) for a single droplet or isolated particle was used (Negiz et al., 1995; Pinto et al., 2014):

$$Nu = \frac{\alpha d_p}{k_a} = 2 + 0.6 Re^{0.5} Pr^{0.33} \tag{8}$$

with

$$Re = \frac{\rho_a d_p}{\mu_a}(v_p - v_a) \tag{9}$$

$$Pr = \frac{cp_a \mu_a}{k_a} \tag{10}$$

being μ_a, cp_a and v_a the viscosity, specific heat capacity and superficial velocity of the air, respectively. The air velocity is estimated from the total air mass flowrate ($\dot{M}_a$), the chamber cross sectional area and the air density. All properties of the air are calculated as a function of the air temperature (T_a) and estimated from Welty et al. (2008), as well as the D_{eff} that is computed at 298 K.

Eq. (4) is evaluated until the particle reaches the equilibrium moisture content (W_{peq}), which is the minimum amount of water that the particle can contain at the prevailing drying conditions. Beyond this point the rate of evaporation becomes zero and $W_p = W_{peq}$. As it will be explained later, W_{peq} is typical of each material, has to be determined experimentally and depends on the drying air relative humidity.

The energy balance for a droplet of mass m_s is:

$$\frac{dT_p}{dz} = \frac{\pi d_p^2[\alpha(T_a - T_p) - \dot{m}_v \Delta H_{ev}]}{v_p m_s(cp_s + W_p cp_w)}, \quad T_p(0) = T_{p0} \tag{11}$$

where T_p is the droplet temperature, ΔH_{ev} and cp_w are the water latent heat of vaporization and the heat capacity of liquid water, respectively (both estimated as a function of T_p from Welty et al. (2008)) and cp_s is the heat capacity of the solid.

Regarding the droplet diameter (d_p) and density (ρ_p), both variables are subjected to change due to the different stages in the evaporation process. In the first stage the droplet shrinks and the density increases as the rate of evaporation is balanced with the transfer of moisture from the centre to the surface of the droplet. The second drying stage starts when the droplet reaches its critical moisture content (W_{pc}) and turns into a wet particle, initiating the formation of a dry porous crust at the droplet surface. In this second stage, moisture is still evaporated from the interior of the droplet, but the diameter of the created particle remains constant and the density starts to decrease. From this point onwards, and until the moisture content reaches the W_{peq}, the transport of water from the inner of the drying droplet to its outer surface becomes the rate-limiting step (Negiz et al., 1995).

Consequently, when $W_p \geq W_{pc}$:

$$\frac{dd_p}{dz} = \frac{d_{p0}\dot{m}_v \pi d_p^2}{3 m_s v_p}\left(\frac{\rho_{p0} - \rho_w}{\rho_p - \rho_w}\right)^{-2/3}\left(\frac{\rho_{p0} - \rho_w}{\rho_p - \rho_w}\right)^2 \rho_s \frac{1 - \frac{\rho_s}{\rho_w}}{\left(1 + \frac{\rho_s}{\rho_w} W_p\right)^2}, \quad d_p(0) = d_{p0} \tag{12}$$

$$\frac{d\rho_p}{dz} = -\frac{\dot{m}_v \pi d_p^2 \rho_s}{m_s v_p}\frac{1 - \frac{\rho_s}{\rho_w}}{\left(1 + \frac{\rho_s}{\rho_w W_p}\right)^2}, \quad \rho_p(0) = \rho_{p0} \tag{13}$$

when $W_{peq} < W_p < W_{pc}$:

$$\frac{dd_p}{dz} = 0 \tag{14}$$

$$\frac{d\rho_p}{dz} = -\frac{6\dot{m}_v}{d_p v_p} \tag{15}$$

and when $W_p < W_{peq}$:

$$\frac{d\rho_p}{dz} = 0 \tag{16}$$

ρ_{p0} is estimated from the solid density (ρ_s) and water density (ρ_w) taking into account the liquid feed solid concentration, and d_{p0} constitutes the droplet mean size estimated from Eq. (1). Regarding the rate of evaporation, it is estimated by means of Eq. (5), which is acceptable as the critical moisture content is close to the equilibrium one (see Section 4).

The change in the velocity of the droplet (v_p) is estimated through its momentum balance. The net forces acting on the droplet constitute the downward gravity force, the upward friction and buoyancy forces. The resulting net force is balanced with the acceleration of the droplet giving:

$$\frac{dv_p}{dz} = g\left(\frac{\rho_p - \rho_a}{\rho_p v_p}\right)^{-3/4} - \frac{3}{4}\frac{C_D \rho_a}{d_p \rho_p v_p}(v_a - v_p)^2, \quad v_p(0) = v_{p0} \tag{17}$$

where g is the acceleration of gravity and C_D is the drag coefficient, that for laminar regime and a spherical droplet is estimated as follows:

$$C_D = \frac{24}{Re} \tag{18}$$

2.2.2. Gas phase balances

The mass balance for the air moisture content is given as:

$$\frac{dY_b}{dz} = N_t \frac{\dot{m}_v \pi d_p^2}{\dot{M}_a v_p}, \quad Y_b(0) = Y_{b0} \tag{19}$$

The initial moisture content (Y_{b0}) is estimated from the ambient air relative humidity, $\dot{M}_a$ represents the dry air mass flowrate (drying and atomization air) and N_t is the total number of droplets that enter the chamber, which can be calculated as:

$$N_t = \frac{\dot{M}_l}{V_{p0}\rho_{p0}} \tag{20}$$

where $\dot{M}_l$ is the liquid feed mass flowrate and V_{p0} represents the droplet initial volume, estimated from Eq. (1) considering an spherical droplet.

The energy balance for the drying medium is given as:

$$\frac{dT_a}{dz} = -\frac{N_t \pi d_p^2 (\dot{m}_v \overline{cp}_v + \alpha)(T_a - T_p)}{v_p \dot{M}_a (cp_a + X_b cp_v)} + \frac{U(T_a - T_p)\pi D_c}{\dot{M}_a (cp_a + X_b cp_v)}, \quad T_a(0) = T_{a0} \tag{21}$$

U represents the global heat transfer coefficient, which accounts for the loss due to conduction through the chamber wall:

$$\frac{1}{U} = \frac{d_v}{k_v} + \frac{d_{air}}{k_a} \tag{22}$$

here d_v is the chamber wall thickness, k_v and k_a the glass and air thermal conductivity respectively, and d_{air} is the boundary layer thickness of the surrounding air, which as cannot be measured is a fitting parameter of the model (Grasmeijer et al., 2013). The initial air temperature T_{a0} is estimated considering the inlet temperature of both, drying and atomizing air, D_c is the diameter of the chamber and $\overline{cp}_v$ is the heat capacity of vapour evaluated as:

$$\overline{cp}_v = \frac{1}{T_p - T_a} \int_{T_a}^{T_p} cp_v dT \tag{23}$$

3. Materials and methods

3.1. Spray drying experimental design

In order to test the validity of the proposed model, a series of experiments were carried out. In particular, aqueous solutions of ciprofloxacin hydrochloride were dried by using a Mini Spray Dryer B-290 (BÜCHI, Flawil, Switzerland) equipped with a high performance cyclone. A standard 0.7 mm two-fluid nozzle was used. The drying air volumetric flowrate was set at 100% of aspiration for the totality of the performed runs. The remaining process parameters were set according to the selected factorial design.

The design of experiments used was a 2^{4-1} fractional factorial design with central point. The statistical analysis was carried out with the assistance of Design Expert software (version 7.0.0). Based on the results of preliminary trials and data reported in the literature, the selected factors were ciprofloxacin hydrochloride concentration (C, mg/mL), drying air inlet temperature (T_{ad}, °C), feed volumetric flowrate (F_l, mL/min) and atomization air volumetric flowrate (F_{at}, NL/h). Each factor was studied at a low, medium and high level, as listed in Table 1. All the runs were performed in duplicate and in a randomized manner to eliminate any unknown possible sources of bias.

During each run, the outlet temperature sensed by the spray-dryer thermocouple was registered (located in the connection between the drying cylinder and the cyclone, see Fig. 1a) as well as ambient temperature (T_{amb}) and relative humidity (RH). Furthermore, the following determinations were carried out for characterizing the atomizing solution and the dried product:

(a) CIP solutions kinematic viscosity, density and surface tension.
The viscosity was determined at 25 °C, using a capillary Cannon Flenske Routine-type viscometer (Tube size 100, IVA, Cannon Instrument Company, State College, United States). Density was calculated by using a 25 mL pycnometer, also performed at 25 °C. Surface tension was measured with a ring Krüss tensiometer (Krüss GmbH, Hamburg, Germany) at room temperature. All determinations were carried out in triplicate.

(b) Moisture content.
The moisture content of the obtained particles was determined by using a halogen moisture analyzer (MB45, Ohaus, Pine Brook, United States). Around 500 mg of sample were heated up to 80 °C until the weight change was less than 1 mg in 90 s. These determinations were carried out immediately after the spray drying process.

(c) Particle size analysis.
The particle size distribution of the spray-dried particles was determined by laser diffraction on the LA 950V2, Horiba (Kyoto, Japan). Particles were dispersed in lactose (lactose:sample 4:1) to improve the powder flow from the feed hopper to the measuring cell (Ceschan et al., 2015).

(d) Skeletal density determination.
The sample or skeletal density of the spray-dried particles was determined by nitrogen adsorption (Nova 1200e, Quantachrome Instruments, Florida, United States). 1 g sample was placed in a precalibrated cell and its volume was determined by nitrogen intrusion. The sample density was calculated as the solid mass divided by the volume of the particles excluding the open pores. Therefore, for non-porous particles or open porous particles the sample density can be assumed to be close to the solid density (ρ_s), while for particles with internal porous the sample density represents the particle density (ρ_p) (Ceschan et al., 2015).

(e) Estimated aerodynamic diameter.
The particle size of drugs for inhalatory applications is critical for its efficient deposition in the lower airways. In fact, the efficacy of the drug product is determined by the amount of drug with aerodynamic particles sizes of a particular size range (i.e., typically <5–10 μm and is usually referred to as the respirable dose) (Van Oort, 1995). The aerodynamic diameter (d_{aer}) of each sample was estimated from its respective d_{43} (mean volumetric diameter) and particle relative density ($\rho_{p,R}$), as follows (Ceschan et al., 2015):

$$d_{aer} = d_{43}\sqrt{\rho_{p,R}} \tag{24}$$

where $\rho_{p,R} = \rho_p/(1000\,kg/m^3)$.

3.2. Droplet size measurement

In order to determine the droplet size generated in the spray-dryer nozzle, different atomizing experiments were carried out using pure water and aqueous solutions of CIP of 10 mg/mL and 50 mg/mL. The nozzle used for atomization was the externally mixing two-fluid nozzle provided with the spray dryer B-290 that has a 0.7 mm liquid orifice diameter (d_L), a 1.1 mm liquid outer diameter ($d_{L,ext}$) and a 1.5 mm gas orifice diameter (d_{air}). The liquid to be atomized was transported up to the atomizing system by means of a peristaltic pump (Masterflex easy-load 7518-00, Cole Palmer). The air flowrate was determined by a rotameter (Brooks Instruments, The Netherlands)

Table 1 – Process variables used in the experimental design.

Factors	Low (–)	Medium (0)	High (+)	Units
CIP concentration	10	30	50	mg/mL
Inlet temperature	110	145	180	°C
Feed volumetric flowrate	3.0	4.5	6.0	mL/min
Atomization air volumetric flowrate	667	1020	1374	NL/h

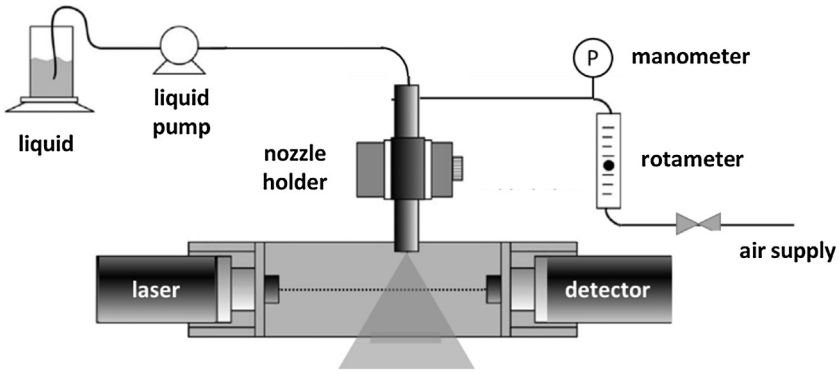

Fig. 2 – Schematic representation of the set up for the droplet size measurement.

and the pressure was registered with a manometer installed in the rotameter (see Fig. 2).

The droplets size was measured by laser diffraction with an Insitec Spray device (Malvern, United Kingdom), having a particle size range of 0.1–2500 μm. It allows in situ, real-time particle size measurement for sprays and aerosols. The nozzle was positioned perpendicular to the laser beam, as shown in Fig. 2. The distance between the nozzle exit and this latter was set to 10 cm. The software RT Sizer (Malvern, United Kingdom) was used to register the data and calculate the Sauter mean droplet diameter.

All the experiments were carried out at ambient conditions, with the same nozzle and at constant liquid feed rate ($\dot{M}_l$). The air feed flowrate ($\dot{M}_a$) was varied in order to test the dependence of the droplet size with the ALR.

3.3. *Determination of the drying air aspirator performance curve*

In order to determine the aspirator performance curve and obtain the relationship between the aspirator setting and the drying air mass flowrate, different experiences were carried out by measuring the velocity of the air at the sprayer exit with a pitot tube connected with a manometer of double reading (CEM Instruments, Shenzhen, China). By registering the air velocity, pressure and temperature at different aspirator settings it was possible to build the performance curve (i.e., mass flowrate versus aspirator setting).

3.4. *Determination of heat transfer coefficient for conduction losses*

According to the proposed energy balance for the air phase (Eq. (21)), it is necessary to determine the thickness of the boundary layer of the surrounding air (d_{air}). To this end, different experiments were carried out in the spray dryer varying the temperature of the drying air (T_{a0}) within the range of the experimental design. All other variables were kept constant: the aspirator setting was established in 100%; the atomization air flowrate and the liquid feed were set in intermediate values, 1052 NL/h and 3 mL/min, respectively. Pure water was

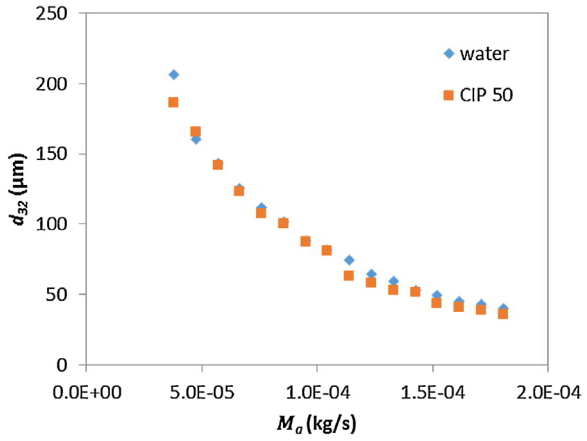

Fig. 3 – Mean droplet diameter for pure water and 50 mg/mL CIP solution.

atomized as a model system, taking into account that it is one of the most common solvents. During each run, the outlet temperature sensed by the spray-dryer thermocouple was registered as well as ambient temperature (T_{amb}) in order to further perform the parameter fitting.

4. Results

4.1. *Atomization model*

As described in Section 3.2, different atomization runs were carried out in order to determine the best fit of Eq. (1). Three runs were performed with pure water, one run with an aqueous CIP solution of 10 mg/mL and one run with an aqueous CIP solution of 50 mg/L. In each run, the ALR was varied from 0.5 to 2.5 approximately, according to the capacity of the rotameter and peristaltic pump available for the experiments. As an example, Fig. 3 shows the d_{32} evolution for one run with pure water and one with the most concentrated CIP solution. As it can be seen, both runs present similar mean droplet size vs. ALR trends, indicating that the Sauter diameter is almost independent of the CIP concentration. This is expected because, as shown in Table 2, CIP aqueous solutions have values of density,

Table 2 – Water and CIP aqueous solutions density, viscosity and superficial tension.

	ρ_L (g/mL)	μ_L (mm^2/s)	γ_L (mV/m)
Water	0.997	1.415	69.6
CIP 10	1.000	1.464	65.8
CIP 50	1.013	1.579	63.0

viscosity and surface tension very similar to water. Therefore, Eq. (1) becomes only dependent on the ALR settings since the liquid orifice (d_L) is the same for all runs and the air properties do not vary. It is important to note that for high ALR values, the mean droplet diameter evolves asymptotically to a constant value.

According to these observations, two runs performed with water were used for parameter fitting and the remaining run with water and the two runs with CIP solutions were saved for validating the model. Because of the constant liquid properties, the *Oh* number is the same for all the performed experiments, therefore the parameters to be fitted in Eq. (1) can be reduced to two: A' and B, where $A' = 1 + C\,\mathrm{Oh}$ and Eq. (1) becomes:

$$d_{32} = A' d_L \left[\frac{\mathrm{We}}{\left(1 + \frac{1}{\mathrm{ALR}}\right)^2} \right]^B \tag{25}$$

Eqs. (25), (2) and (3) were implemented in the gPROMS Environment (gPROMS, 2016) and the fitting parameters were estimated from experimental data using the inbuilt parameter estimation tool. As a result, $A' = 0.3771$ and $B = -0.3487$, which are within the ranges reported for this type of nozzles (Walzel, 2012). Furthermore, Table 3 presents the statistical analysis performed by gPROMS, showing a t-value much larger than the reference t-value that indicates high accuracy of the estimated parameter, and a weighted residual smaller than χ^2 value, which indicates that a large amount of the variance in the data can be explained by the model (gPROMS, 2016).

In order to test the validity of the correlation in systems that were note used for the parameter fitting, Fig. 4 shows the predicted d_{32} together with the experimental measurements for one run performed with pure water and the two runs with CIP solutions. As it can be seen, the predictions are in reasonable accordance with the experimental observations.

4.2. *Heat transfer coefficient*

In order to obtain d_{air} the experiments shown in Table 4 were performed. The first three runs were used to estimate d_{air}, which resulted in a value of 8.97E−4 m. Due to its simplicity, the parameter estimation was performed by means of the Excel Solver tool. With the remaining tests, the validity of the model was evaluated considering that a different liquid flowrate was assayed. As it can be seen, the coefficient of determination is equal to 0.95, showing a reasonable prediction.

4.3. *Drying model*

4.3.1. *Parameter fitting*

The validity of the proposed model was tested by simulating the experimental runs described in Table 1. On overall, 9 experiments with their replicates were simulated (i.e., 18 experiments). The spray-dryer model was implemented in the gPROMS Environment considering as input for each run the data presented in Table 1 (i.e., CIP concentration, drying air inlet temperature, feed flowrate and atomization air flowrate), the ambient temperature and relative humidity, the mean droplet size correlation presented in Section 4.1 and the heat transfer coefficient fitted in Section 4.2. The model also requires as inputs the particles' critical and equilibrium moisture content as well as CIP properties.

Regarding the W_{peq} (minimum amount of water that the particle can contain at the prevailing drying conditions) it was determined from the dynamic vapour sorption (DVS) isotherms of spray-dried ciprofloxacin hydrochloride performed by Ong et al. (2011) and Adi et al. (2008). As stated by the authors, each sample was dried at 0% RH before being exposed to 10% RH increments at 25 °C. Equilibrium moisture content at each increment was determined by dm/dt of 0.002% min^{-1}. Fig. 5a presents a cycle of sorption and desorption obtained from these authors. Specifically, CIP particles had a large hysteresis between the sorption and desorption cycles. As stated by Young et al. (2014): "during the first sorption cycle, an increase in mass of ≈11% was observed, between 0 and 60% RH, before water was expelled at 70% RH, indicating an amorphous-crystalline transition. The mass loss on desorption did not return to 0% but rather 4%, indicating that significant water was retained in the crystallized sample".

Strictly, W_{peq} has to be determined from desorption cycles as the process under study is a drying operation. However, according to our experimental evidence: (a) CIP particles leave the spray dryer with a moisture content between 1.21 and 4.57 (wt%) and (b) X-ray Diffraction tests indicate that particles both in amorphous and crystalline state have been produced. Taking into account these facts and in order to allow W_{peq} to reach even the lowest moisture content values experimentally found, W_{peq} was obtained from the sorption isotherm. Fig. 5b presents the equilibrium values (kg of water/kg of CIP) from which a correlation to estimate W_{peq} as a function of the air RH was obtained: $W_{peq} = (\%\ \mathrm{w/w})/100$.

With respect to the W_{pc} (moisture content for the formation of a dry porous crust at the droplet surface), its determination is quite more challenging as it depends on the particle drying kinetics and is usually set as a model fitting parameter (Negiz et al., 1995). For this contribution, and taking into account that in a drying process W_{pc} is higher than W_{peq}, the critical moisture content was assumed as 30% higher than the equilibrium one.

Both W_{pc} and W_{peq} are function of the drying air RH. Since this air is changing its temperature along the dryer, the RH, which in the model is estimated through Eq. (26), also varies:

$$\mathrm{RH} = \frac{1}{\frac{1}{Y_B}\frac{\tilde{M}_w}{\tilde{M}_a} + 1} \frac{P}{P_v(T_a)} \tag{26}$$

This change is considered until W_p equals W_{peq}, from this point onward the RH is kept in its last value.

Regarding the ciprofloxacin properties, its heat capacity was set in $cp_s = 56.8$ J/kg K (Zhang, 2005) and the solid density was inferred from the obtained skeletal values. Taking into account the measured particle moisture content and assuming that the highest value of skeletal density corresponds to a particle that either has all the porous connected to the surface or the minimum experimental porosity, ρ_s was set as 1300 kg/m^3.

Once all the input variables were determined, the simulation results were compared with the experimental measurements. Among all the variables that define product

Table 3 – Statistical information for the mean droplet size fitting.

Parameter	Final value	95% t-value	Std. dev.	Ref. t-value (95%)	Weighted residual	χ^2 value (95%)
A	0.3771	9.4	0.0187	1.7612	17.929	23.685
B	−0.3487	9.1	0.0179			

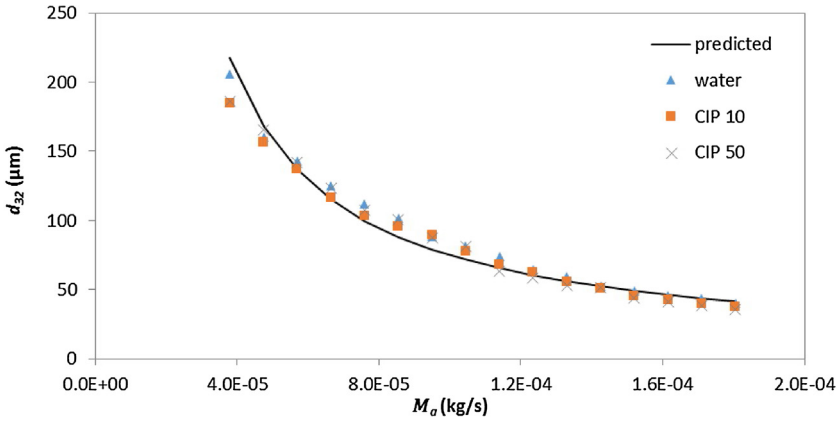

Fig. 4 – Predicted and experimental d_{32} for pure water and CIP solutions of 10 mg/mL and 50 mg/mL.

Table 4 – Heat transfer coefficient experimental data and coefficient of determination.

F_l, (mL/min)	$\dot{M}_{ad}$ (kg/s)	T_{ad} (°C)	T_{out} (°C)	T_{amb} (°C)	$\dot{M}_{aat}$ (kg/s)	T_{a0} (°C)	T_{out} pred. (°C)	R^2
3	8.5E−3	110	57	27.2	3.9E−4	106.35	56.11	0.99
3	8.5E−3	145	69	27.1	3.9E−4	139.81	70.16	
3	8.5E−3	180	85	27.1	3.9E−4	173.26	83.39	
4.5	8.5E−3	110	48	27.2	3.9E−4	106.35	52.43	0.95
4.5	8.5E−3	145	64	27.1	3.9E−4	139.82	66.74	
4.5	8.5E−3	180	79	27.2	3.9E−4	173.27	80.33	

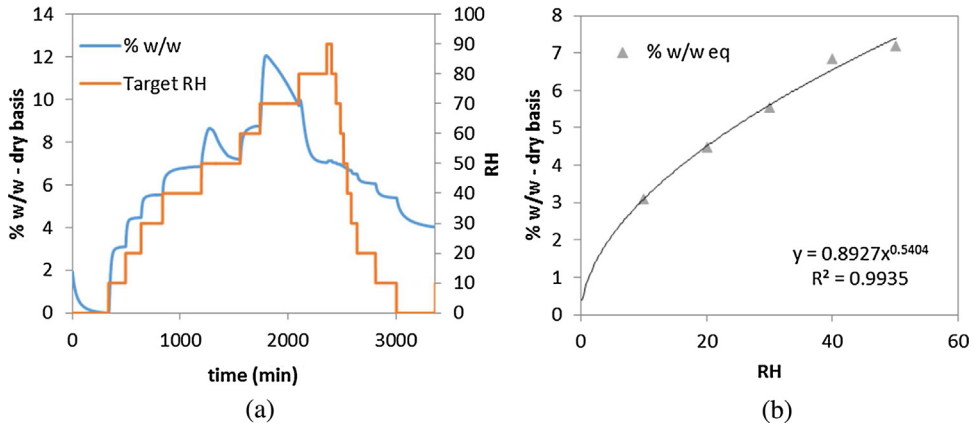

Fig. 5 – (a) CIP DVS from Ong et al. (2011) and Adi et al. (2008). (b) Correlation to estimate W_{peq}.

quality, particle size, particle density, moisture content and outlet temperature are the ones that the proposed model allows to predict.

Regarding the particle size, Fig. 6a shows the values predicted by the model against the experimental data. Firstly, it is good to note that the experimental information is highly replicable as the highest value for the standard deviation is 6E−7 m (i.e., low error bars). As it can be seen in Fig. 6a, the predicted mean size follows quite well the experimental ones: the highest experimental values (runs 3 and 7) are also the highest predicted values; the lowest experimental values (runs 2, 4 and 6) are within the lowest predicted ones, except for predicted run 1. From Fig. 6b, it can be seen that the manipulated variables that more influence the predicted values (and possible, the experimental ones) are the droplet size and solid concentration. Runs 3, 5, 6 and 7 present the highest droplet size, although run 5 and 6 present the lowest concentration giving a smaller predicted (and experimental) particle size. Runs 1, 2, 4 and 8 present the lowest droplet size, consequently the predicted and experimental particle size are within the lower ones, except that runs 2 and 8 present the highest concentration and therefore, their predicted size are higher than the other two. Run 9 presents and intermediate combination and, consequently, predicted and experimental particle sizes are midway.

Fig. 7 presents the experimental and predicted particle (or skeletal) density. It can be seen that although the simulated density is always overestimating the experimental data, it follows the behaviour between runs, with errors smaller than 6.4%. The fact that the experimental values are smaller than the predicted ones can be indicating that the particles are porous inside and, therefore, their density is smaller than

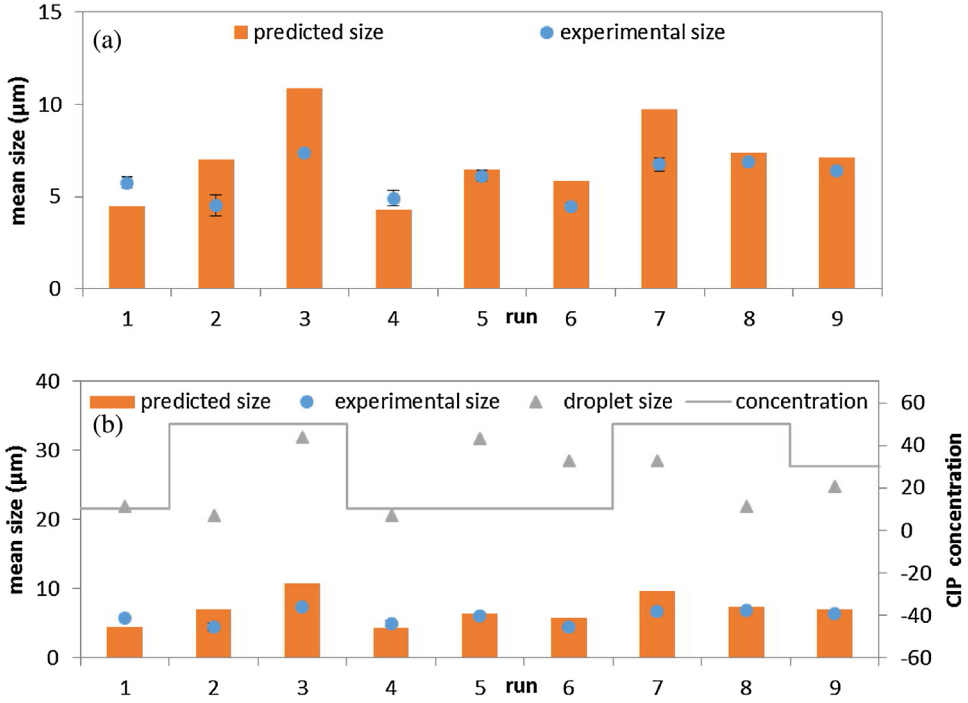

Fig. 6 – Experimental and predicted particle size.

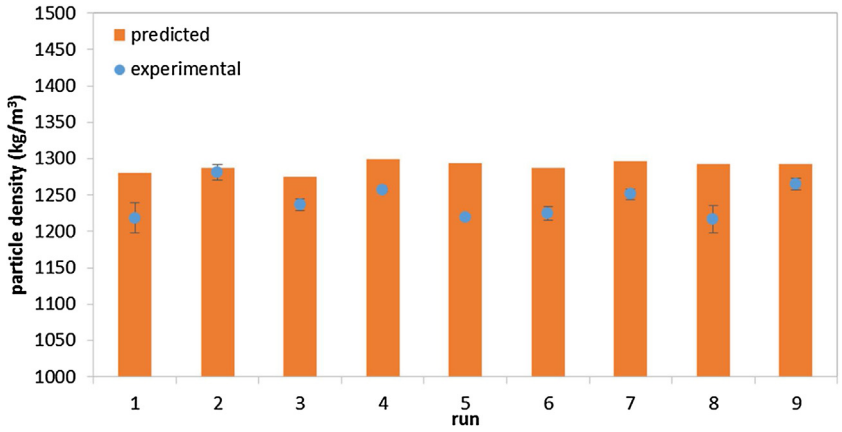

Fig. 7 – Experimental and predicted particle density.

the solid one. The model (as it is presented in this contribution) does not include the prediction of particle porosity; this should be taken into account in future improvements of this simulation tool. In fact, previous authors have described solid formation inside droplets by the solution of population balances. Seydel et al. (2006) described the crystallization process and the distribution of particles (and voids) in the drying of solution droplets. Handscomb et al. (2009b) and Bück et al. (2012) used the same approach to model aggregation of nanoparticles when drying single suspension droplets. Regarding the experimental particle density values, it is noted that the replicates present small variations between them, with standard deviation values smaller than 21.21 kg/m^3.

Fig. 8 shows the predicted and experimental values (as water mass fraction) for the particle moisture content after the spray drying. Unlike the particle diameter and density, the moisture content presents more variability between replicates (high error bars), with standard deviations lower than 0.013% (wt/wt). For all runs, except run 3, the predicted moisture content underestimates the experimental value. This could be related to the estimation of the equilibrium particle moisture (W_{peq}) by means of the sorption isotherm instead of the desorption one. Moreover, it could be a consequence of the model hypothesis (f) and of considering plug flow for the air and droplet's phases which implies a higher residence time that the one observed by other authors (Pinto et al., 2014). Nonetheless, the highest difference between model predictions and experimental values is 2.4% (wt/wt) with an average deviation of 1.1% (wt/wt), which can be considered reasonable. Besides, it also should be taken into account that the moisture content experimental value is highly dependent on the quality of the measurement. Although the determinations were carried out immediately after the spray drying process, there might be some effect related to ambient moisture intake by the particles.

Fig. 9 presents the predictions of the air outlet temperature against the experimental values. As it can be seen, the model captures very well the real process. The predicted values show the same behaviour between runs as the experimental ones. In fact, the highest error is 12% with an average value of 7%. Deviations between replicates in each run are reasonable, being the highest 8.8 °C.

On overall, the predictions made by the model are satisfactory taking into account that the droplet size distribution and

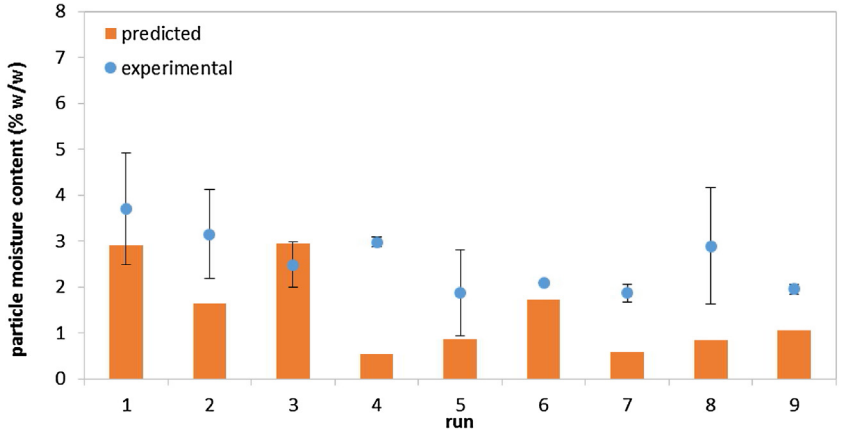

Fig. 8 – Experimental and predicted particle moisture content.

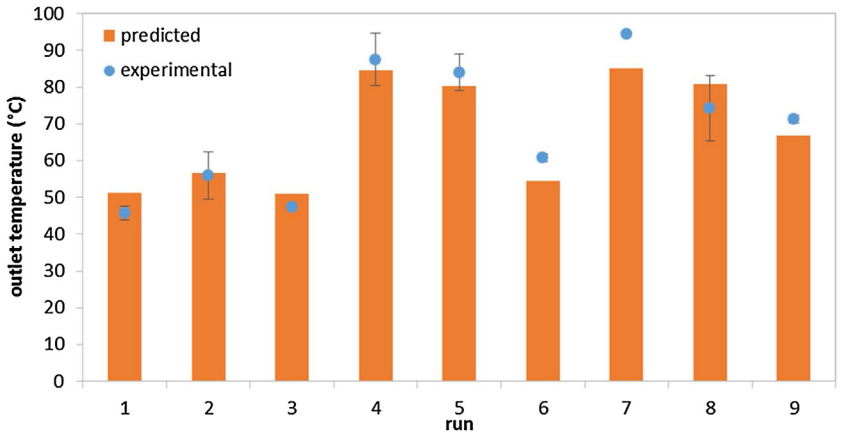

Fig. 9 – Experimental and predicted outlet air temperature.

the convective heat loss are the only variables that present fitted parameters and have been determined for the specific nozzle and spray dryer used in this contribution but for a common system as pure water.

In order to identify if the particle size and density can be improved by better estimating the W_{pc}, a sensitivity analysis with respect to this variable was performed. Run 3 was chosen as the base case for the sensitivity analysis since it presents the worst prediction of the particle size. Fig. 10 shows the evolution along the spray drier of the described variables for the base case, a simulation with W_{pc} twice the base case and a simulation with W_{pc} ten times the base case. As it can be seen in Fig. 10a, the particle size increases as the critical moisture content increases, which makes sense since the point of crust formation is at shorter lengths. These results are worse than the prediction obtained for the base case in Run 3. Indeed, it is expected that all the particle size predictions increase their values as the W_{pc} increases. Comparing with Fig. 10b, the effect of changing W_{pc} on the particle density is much pronounced. As the critical moisture is reached at shorter distances from the nozzle, the second stage of drying is longer, and therefore, evaporation continues with a constant particle diameter. This disturbance leads to a lower particle density than the base case. Consequently, a higher W_{pc} can result in better predictions of the particle density. From Fig. 10c and d it can be seen that changes in W_{pc} do not affect the evolution of the particle and air temperatures as well as the particle final moisture content, which depends on the equilibrium moisture content.

From the sensitivity analysis it can be inferred that the W_{pc} estimation can be critical in improving the prediction of the particle density. Nonetheless, as afore-mentioned, the model needs to be updated in order to take into account that the particles can have internal porous. In contrast, the particle size is more susceptible to a good prediction of the droplet size than to the estimation of the critical moisture content.

Table 5 – Experimental and predicted aerodynamic diameter.

Run	d_{aer} (μm) experimental	d_{aer} (μm) predicted
1	6.35	5.04
2	5.13	7.94
3	8.18	12.26
4	5.50	4.85
5	6.76	7.32
6	4.95	6.63
7	7.53	11.05
8	7.58	8.37
9	7.19	8.11

Finally, for the produced particles to be used as inhalable powder, the aerodynamic diameter needs to be below 10 μm. Table 5 presents the d_{aer} calculated by Eq. (24) from the experimental and predicted data. For the experimental data, it is verified that in all cases the particles are below the maximum allowable diameter. For the predicted data, as the particle density is over-predicted and in some cases the particle size too, runs 3 and 7 fall outside the limit. Nonetheless, this result implies that the developed model can be used with confidence to determine the combination of operating variables that allow the production of inhalable particles by spray drying.

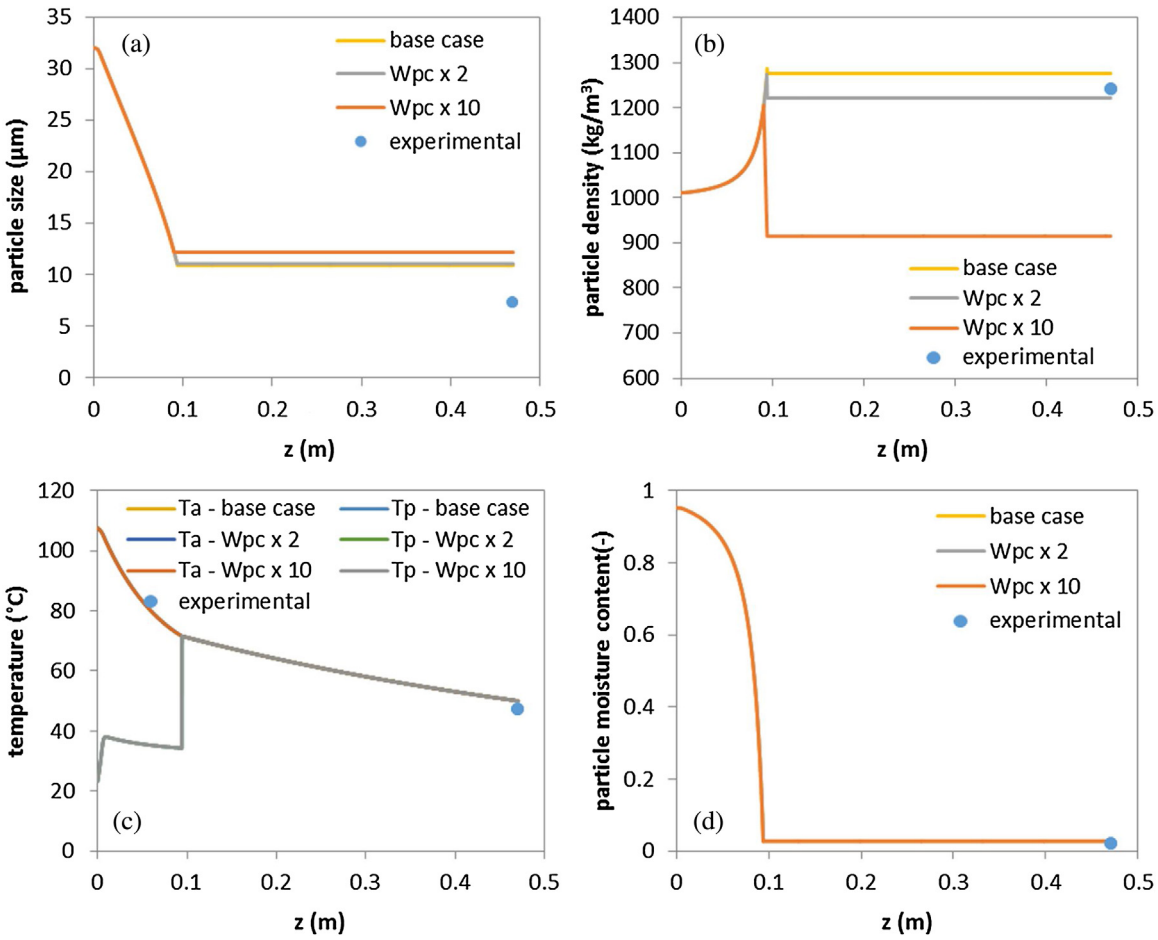

Fig. 10 – W_{pc} sensitivity analysis.

5. Conclusions

In this contribution and with the aim of providing a simulation tool for the design of inhalable particles, experimentation and modelling were combined to represent a spray dryer operation. The model, that describes variations in the axial direction of mean droplet/particle size, droplet and air temperature, droplet and air moisture and droplet and air velocity, involves the determination of unknown fitting parameters associated with the mean droplet size generated in the dryer nozzle and the heat transfer to the environment. These were determined through experiments based on a simple system like pure water, providing a model capable of predicting satisfactorily the main operating variables and product quality parameters. Furthermore, the proposed model was validated with data provided by a design of experiments that allowed proving its performance in a wide range of operating and formulation conditions.

The results suggest that the predictions of particle density could be improved if the porosity of the particles and their changes throughout the drying process are considered. On the other hand, the predicted final moisture content of the particles could be optimized by performing DVS assays under conditions similar to those in the spray-drying operation. It was also demonstrated that a good prediction of droplet size is critical for simulating and controlling the particle diameter. As the minimum particle size is limited by the critical moisture content, the evaporation that takes place during the second drying stage does not affect the final particle size. Therefore, if a different product particle size is required, the droplet size and/or solid concentration should be modified. These changes can be achieved by manipulating the atomization air flowrate and the concentration of the feed solution.

Finally, further work will involve, besides the modelling of the intra-particle phenomenon in order to estimate porosity, the inclusion of a droplet size distribution generated in the nozzle as a way to track different fractions of particles along the unit (i.e., fraction of respirable particles, fines recovery) and the evaluation of other process parameters such as yield.

Acknowledgements

The authors express their gratitude for the financial support by the Consejo Nacional de Investigaciones Científicas y Técnicas (CONICET), Agencia Nacional de Promoción Científica y Tecnológica (ANPCyT) and Universidad Nacional del Sur (UNS) of Argentina. M. Razuc thanks CONICET for her posdoctoral fellowship. The authors also thank Mikel Leturia and Khashayar Saleh (UTC; Compiegne, France) for their technical assistance in the droplet size measurements, Paul Young (Woolcock Institute of Medical Research; Sidney, Australia) for the provided experimental information and Fernanda Cabrera (PLAPIQUI-CONICET) for her technical assistance.

References

Adi, H., Young, P.M., Chan, H.-K., Agus, H., Traini, D., 2010a. Co-spray-dried mannitol-ciprofloxacin dry powder inhaler formulation for cystic fibrosis and chronic obstructive

pulmonary disease. Eur. J. Pharm. Sci. 40, 239–247, http://dx.doi.org/10.1016/j.ejps.2010.03.020.
Adi, H., Young, P.M., Chan, H.-K., Salama, R., Traini, D., 2010b. Controlled release antibiotics for dry powder lung delivery. Drug Dev. Ind. Pharm. 36, 119–126, http://dx.doi.org/10.1002/jps.21239.
Adi, H., Young, P.M., Chan, H.-K., Stewart, R., Agus, H., Traini, D., 2008. Cospray dried antibiotics for dry powder lung delivery. J. Pharm. Sci. 97, 3356–3366, http://dx.doi.org/10.1002/jps.
Balliu, N., 2005. An Object Oriented Approach to the Modelling and Dynamics of Granulation Circuits.
Bell, T., 2005. Challenges in the scale-up of particulate processes: an industrial perspective. Powder Technol. 150, 60–71, http://dx.doi.org/10.1016/j.powtec.2004.11.023.
Boukouvala, F., Chaudhury, A., Sen, M., Zhou, R., Mioduszewski, L., Ierapetritou, M.G., Ramachandran, R., 2013. Computer-aided flowsheet simulation of a pharmaceutical tablet manufacturing process incorporating wet granulation. J. Pharm. Innov. 8, 11–27, http://dx.doi.org/10.1007/s12247-012-9143-9.
Bück, A., Peglow, M., Naumann, M., Tsotsas, E., 2012. Population balance model for drying of droplets containing aggregating nanoparticles. AIChE J., 1–11, http://dx.doi.org/10.1002/aic.
Burggraeve, A., Monteyne, T., Vervaet, C., Remon, J.P., Beer, T.D., 2013. Process analytical tools for monitoring, understanding, and control of pharmaceutical fluidized bed granulation: a review. Eur. J. Pharm. Biopharm. 83, 2–15, http://dx.doi.org/10.1016/j.ejpb.2012.09.008.
Ceschan, N.E., Bucalá, V., Ramírez-Rigo, M.V., 2015. Polymeric microparticles containing indomethacin for inhalatory administration. Powder Technol. 285, 1–11, http://dx.doi.org/10.1016/j.powtec.2015.02.001.
Christofides, P.D., El-Farra, N.H., Li, M., Mhaskar, P., 2008. Model-based control of particulate processes. Chem. Eng. Sci. 63, 1156–1172, http://dx.doi.org/10.1016/j.ces.2007.07.017.
Christofides, P.D., Li, M., Mädler, L., 2007. Control of particulate processes: recent results and future challenges. Powder Technol. 175, 1–7, http://dx.doi.org/10.1016/j.powtec.2007.01.021.
Dobry, D.E., Settell, D.M., Baumann, J.M., Ray, R.J., Graham, L.J., Beyerinck, R.A., 2009. A model-based methodology for spray-drying process development. J. Pharm. Innov. 4, 133–142, http://dx.doi.org/10.1007/s12247-009-9064-4.
Edrisi Sormoli, M., Langrish, T.A.G., 2016. The use of a plug-flow model for scaling-up of spray drying bioactive orange peel extracts. Innov. Food Sci. Emerg. Technol. 37, 27–36, http://dx.doi.org/10.1016/j.ifset.2016.08.004.
Fung, K.Y., Ng, K.M., Nakajima, S., Wibowo, C., 2006. A systematic iterative procedure for determining granulator operating parameters. AIChE J. 52, 3189–3202.
Grasmeijer, N., de Waard, H., Hinrichs, W.L.J., Frijlink, H.W., 2013. A user-friendly model for spray drying to aid pharmaceutical product development. PLoS ONE 8, e74403, http://dx.doi.org/10.1371/journal.pone.0074403.
Halstensen, M., Debakker, P., Esbensen, K., 2006. Acoustic chemometric monitoring of an industrial granulation production process – a PAT feasibility study. Chemom. Intell. Lab. Syst. 84, 88–97, http://dx.doi.org/10.1016/j.chemolab.2006.05.012.
Handscomb, C.S., Kraft, M., Bayly, A.E., 2009a. A new model for the drying of droplets containing suspended solids after shell formation. Chem. Eng. Sci. 64, 228–246, http://dx.doi.org/10.1016/j.ces.2008.04.051.
Handscomb, C.S., Kraft, M., Bayly, A.E., 2009b. A new model for the drying of droplets containing suspended solids. Chem. Eng. Sci. 64, 628–637, http://dx.doi.org/10.1016/j.ces.2008.04.051.
Hede, P., Bach, P., Jensen, A., 2008. Two-fluid spray atomisation and pneumatic nozzles for fluid bed coating/agglomeration purposes: a review. Chem. Eng. Sci. 63, 3821–3842, http://dx.doi.org/10.1016/j.ces.2008.04.014.
Kemp, I.C., Hartwig, T., Hamilton, P., Wadley, R., Bisten, A., 2016. Production of fine lactose particles from organic solvent in laboratory and commercial-scale spray dryers. Dry. Technol. 34, 830–842, http://dx.doi.org/10.1080/07373937.2015.1084314.
Kemp, I.C., Wadley, R., Hartwig, T., Cocchini, U., See-Toh, Y., Gorringe, L., Fordham, K., Ricard, F., 2013. Experimental study of spray drying and atomization with a two-fluid nozzle to produce inhalable particles. Dry. Technol. 31, 930–941, http://dx.doi.org/10.1080/07373937.2012.710693.
Kuriakose, R., Anandharamakrishnan, C., 2010. Computational fluid dynamics (CFD) applications in spray drying of food products. Trends Food Sci. Technol. 21, 383–398, http://dx.doi.org/10.1016/j.tifs.2010.04.009.
Lyu, F., Liu, J.J., Zhang, Y., Wang, X.Z., 2017. Combined control of morphology and polymorph in spray drying of mannitol for dry powder inhalation. J. Cryst. Growth 467, 155–161, http://dx.doi.org/10.1016/j.jcrysgro.2017.03.033.
Maltesen, M.J., Bjerregaard, S., Hovgaard, L., Havelund, S., van de Weert, M., 2008. Quality by design – spray drying of insulin intended for inhalation. Eur. J. Pharm. Biopharm. 70, 828–838, http://dx.doi.org/10.1016/j.ejpb.2008.07.015.
MedlinePlus, 2017. Ciprofloxacina, https://medlineplus.gov/spanish/druginfo/meds/a688016-es.html (accessed 27.07.17).
Mezhericher, M., Levy, A., Borde, I., 2008. Modelling of particle breakage during drying. Chem. Eng. Process. Process Intensif. 47, 1410–1417, http://dx.doi.org/10.1016/j.cep.2007.06.018.
Mezhericher, M., Levy, A., Borde, I., 2010. Theoretical models of single droplet drying kinetics: a review. Dry. Technol. 28, 278–293, http://dx.doi.org/10.1080/07373930903530337.
Negiz, A., Lagergren, E., Cinar, A., 1995. Mathematical models of cocurrent spray drying. Ind. Eng. Chem. Res. 34, 3289–3302.
Ong, H.X., Traini, D., Bebawy, M., Young, P.M., 2011. Epithelial profiling of antibiotic controlled release respiratory formulations. Pharm. Res. 28, 2327–2338, http://dx.doi.org/10.1007/s11095-011-0462-1.
Pacheco, C., Piña, J., Saleh, K., 2016. Molten materials' atomization for particle coating: prediction of mean droplet size for two-fluid nozzles. At. Sprays 26.
Patel, B.B., Patel, J.K., Chakraborty, S., 2014. Review of patents and application of spray drying in pharmaceutical, food and flavor industry. Recent Pat. Drug Deliv. Formul. 8, 63–78.
Patel, K.C., Chen, X.D., 2005. Prediction of spray-dried product quality using two simple drying kinetics models. J. Food Process Eng. 28, 567–594, http://dx.doi.org/10.1111/j.1745-4530.2005.00039.x.
Pinto, M.A., Kemp, I., Bermingham, S., Hartwig, T., Bisten, A., 2014. Development of an axisymmetric population balance model for spray drying and validation against experimental data and CFD simulations. Chem. Eng. Res. Des. 92, 619–634, http://dx.doi.org/10.1016/j.cherd.2013.12.019.
Process System Enterprise, 2016. gPROMS, http://www.psenterprise.com (accessed 08.02.16).
Ranz, W.E., Marshall, W.R., 1952. Evaporation from drops. Parts I & II. Chem. Eng. Prog. 48, 141–146, 173–180.
Schmitz-Schug, I., Kulozik, U., Foerst, P., 2016. Modeling spray drying of dairy products – impact of drying kinetics, reaction kinetics and spray drying conditions on lysine loss. Chem. Eng. Sci. 141, 315–329, http://dx.doi.org/10.1016/j.ces.2015.11.008.
Seydel, P., Blömer, J., Bertling, J., 2006. Modeling particle formation at spray drying using population balances. Dry Technol. 24, 137–146, http://dx.doi.org/10.1080/07373930600558912.
Smith, J.M., Van Ness, H.C., Abbott, M.M., 1997. Introduction to Chemical Engineering Thermodynamics, 5th ed. McGraw-Hill.
Sosnik, A., Seremeta, K.P., 2015. Advantages and challenges of the spray-drying technology for the production of pure drug particles and drug-loaded polymeric carriers. Adv. Colloid Interface Sci. 223, 40–54, http://dx.doi.org/10.1016/j.cis.2015.05.003.
Tran, T.T.H., Jaskulski, M., Avila-Acevedo, J.G., Tsotsas, E., 2017. Model parameters for single-droplet drying of skim milk and its constituents at moderate and elevated temperatures. Dry Technol. 35, 444–464, http://dx.doi.org/10.1080/07373937.2016.1182548.

Tsotsas, E., 2015. Multiscale approaches to processes that combine drying with particle formation. Dry Technol. 33, 1859–1871, http://dx.doi.org/10.1080/07373937.2015.1047954.
Van Oort, M., 1995. In vitro testing of dry powder inhalers. Aerosol Sci. Technol. 22, 364–373, http://dx.doi.org/10.1080/02786829408959754.
Vehring, R., 2007. Pharmaceutical particle engineering via spray drying. Pharm. Res. 25, 999–1022, http://dx.doi.org/10.1007/s11095-007-9475-1.
Vehring, R., Foss, W.R., Lechuga-Ballesteros, D., 2007. Particle formation in spray drying. J. Aerosol Sci. 38, 728–746, http://dx.doi.org/10.1016/j.jaerosci.2007.04.005.
Vicente, J., Pinto, J., Menezes, J., Gaspar, F., 2013. Fundamental analysis of particle formation in spray drying. Powder Technol. 247, 1–7, http://dx.doi.org/10.1016/j.powtec.2013.06.038.
Walzel, P., 2012. Spraying and atomizing of liquids. In: Ullmann's Encyclopedia of Industrial Chemistry. Wiley-VCH Verlag GmbH & Co. KGaA, http://dx.doi.org/10.1002/14356007.b02, 25.1–25.40.
Walzel, P.E., 1993. Liquid atomisation. Int. Chem. Eng. 33, 46–60.
Welty, J.R., Wicks, C.E., Wilson, R.E., Rorrer, G.L., 2008. Fundamentals of Momentum, Heat, and Mass Transfer. Wiley & Sons, http://dx.doi.org/10.1016/0017-9310(70)90063-3.
Young, P.M., Crapper, J., Philips, G., Sharma, K., Chan, H.-K., Traini, D., 2014. Overcoming dose limitations using the Orbital® multi-breath dry powder inhaler. J. Aerosol Med. Pulm. Drug Deliv. 27, 138–147, http://dx.doi.org/10.1089/jamp.2013.1080.
Zbicinski, I., 2017. Modeling and scaling up of industrial spray dryers: a review. J. Chem. Eng. Jpn. 50, 757–767, http://dx.doi.org/10.1252/jcej.16we350.
Zhang, Y., 2005. Screening Method for Evaluation of Bilayer Drug Interaction in Liposomal Compositions, WO2005034915 A2.